


Trigger mechanisms of the major solar flares

Shuhong Yang^{1,2} 

¹CAS Key Laboratory of Solar Activity, National Astronomical Observatories,
Chinese Academy of Sciences, Beijing 100101, China
email: shuhongyang@nao.cas.cn

²School of Astronomy and Space Science, University of Chinese Academy of Sciences,
Beijing 100049, China

Abstract. Solar flares, suddenly releasing a large amount of magnetic energy, are one of the most energetic phenomena on the Sun. For the major flares (M- and X-class flares), there exist strong-gradient polarity-inversion lines in the pre-flare photospheric magnetograms. Some parameters (e.g., electric current, shear angle, free energy) are used to measure the magnetic non-potentiality of active regions, and the kernels of major flares coincide with the highly non-potential regions. Magnetic flux emergence and cancellation, shearing motion, and sunspot rotation observed in the photosphere are deemed to play an important role in the energy buildup and flare trigger. Solar active region 12673 produced many major flares, among which the X9.3 flare is the largest one in solar cycle 24. According to the newly proposed block-induced eruption model, the block-induced complex structures built the flare-productive active region and the X9.3 flare was triggered by an erupting filament due to the kink instability.

Keywords. Sun: atmosphere, Sun: flares, Sun: magnetic fields, Sun: photosphere, sunspots

1. Introduction

Solar flares are one of the most energetic phenomena on the Sun (Priest and Forbes 2002; Benz 2017). During a solar flare, a great amount of energy is released. Magnetic reconnection is deemed to be an efficient way for the sudden release of free energy to drive solar flares and stellar flares (Parker 1957; Rosner *et al.* 1985; Haisch *et al.* 1991; Yang *et al.* 2015). In some flares, a bulk of plasma and magnetic structure can be ejected into the interplanetary space, thus forming a coronal mass ejection (CME; Chen 2011; Schmieder *et al.* 2015; Kilpua *et al.* 2017). CMEs may interact with the Earth and consequently impact on the terrestrial environment and the human activities (Schwenn 2006; Pulkkinen 2007).

Solar flares were first independently discovered in the white light as sudden enhancements of emission in the visible continuum by Carrington (1859) and Hodgson (1859). Actually, solar flares can be observed as conspicuous brightenings in different lines, e.g., H α (see Fig. 1(a)), Ultraviolet (UV), EUV, X-ray, and radio. They have been frequently studied with the space-based instruments (e.g., the Solar and Heliospheric observatory (SOHO; Domingo *et al.* 1995), the Reuven Ramaty High-Energy Solar Spectroscopic Imager (RHESSI; Lin *et al.* 2002), the Hinode (Kosugi *et al.* 2007), the Solar Dynamics Observatory (SDO; Pesnell *et al.* 2012), and the Interface Region Imaging Spectrograph (IRIS; De Pontieu *et al.* 2014)), and the ground-based ones (e.g. the Goode Solar Telescope (GST; former the New Solar Telescope; Cao *et al.* 2010), the Optical and Near-infrared Solar Eruption Tracer (ONSET; Fang *et al.* 2013), the New Vacuum Solar Telescope (NVST; Liu *et al.* 2014), and the MingantU SpEctral Radioheliograph (MUSER; Yan *et al.* 2009; Yan *et al.* 2016; Chen *et al.* 2019)). Although solar flares can

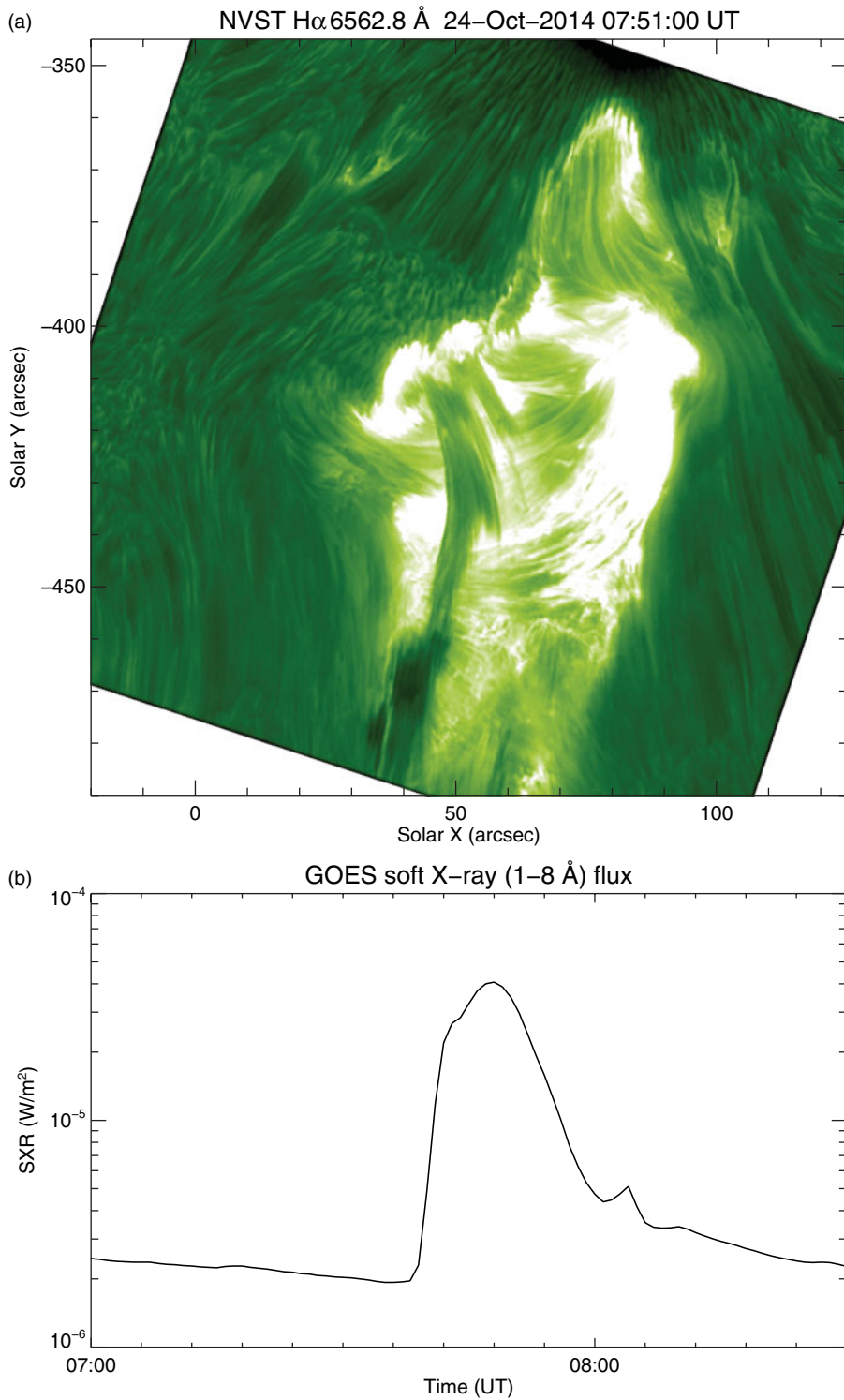


Figure 1. NVST H α 6562.8 Å image (panel (a)) showing an M4.0 flare on 2014 October 24, and the corresponding GOES soft X-ray (1–8 Å) flux variation (panel (b)).

Table 1. Flare classification.

Flare class	A	B	C	M	X
Peak flux ¹ (W/m ²)	<10 ⁻⁷	10 ⁻⁷ – 10 ⁻⁶	10 ⁻⁶ – 10 ⁻⁵	10 ⁻⁵ – 10 ⁻⁴	>10 ⁻⁴

Notes:¹ According to the GOES soft X-ray (1-8 Å) flux.

occur almost everywhere on the Sun, including active regions (ARs) and the quiet Sun, large flares tend to take place in ARs with a complex geometry (Benz & Krucker 1998; Berghmans *et al.* 1998; Régnier & Canfield 2006).

The flare classification uses the letters A, B, C, M and X, according to the peak flux of the Geostationary Operational Environmental Satellite (GOES) soft X-ray (1-8 Å) flux, as shown in Table 1. Fig. 1(b) shows the variation of the soft X-ray 1-8 Å flux corresponding to the M4.0 class flare displayed in Fig. 1(a). Generally, M-class and X-class flares are considered to be major flares.

2. Magnetic properties before major flares

Solar flares tend to occur within ARs with strong magnetic fields and strong field gradients (Jing *et al.* 2006; Wang & Liu 2015; Toriumi & Wang 2019). The separation line between the positive and negative magnetic fields is termed “polarity-inversion line” (PIL; as shown in Fig. 2(a)). Zirin & Wang (1993) investigated the strength and direction of transverse magnetic fields in 6 delta-spots with the spectroscopic measurements. The magnetic fields were found to be parallel to the PIL and the field strengths were as strong as 3980 G. For AR 11035 in 2009 December, Jaeggli (2016) studied the polarized Stokes spectra, and found that the magnetic field near the PIL was strong and nearly horizontal. The largest field strengths were 3500-3800 G. Schrijver (2007) analyzed about 289 major flares, and found that these flares, without exception, were associated with strong-gradient PILs. Toriumi *et al.* (2017) systematically studied 51 flare events with GOES levels larger than M5-class. They found that there were only two flares without strong-gradient PILs. Recently, in a PIL between two opposite-polarity umbrae, Okamoto & Sakurai (2018) reported clear evidence of magnetic field of 6250 G. The strong field was parallel to the solar surface, which was suggested to be generated due to the compression of one umbra pushed by the horizontal flow from the other umbra.

Using the data from the Huairou Solar Observing Station (HSOS) in Beijing, China, Wang *et al.* (1996) studied the relationship between flare occurrence and electric currents. They found that flare activity was closely associated with vertical electric currents. AR 11158 which produced several major eruptions (including the first X-class flare of solar cycle 24) has been extensively studied (e.g., Vemareddy *et al.* 2012; Song *et al.* 2013). Based on the vector magnetograms from the Helioseismic and Magnetic Imager (HMI; Scherrer *et al.* 2012; Schou *et al.* 2012) on board the SDO, Sun *et al.* (2012) studied the magnetic fields of AR 11158 in details and their results revealed that the area with large electric current coincided with the initiation site of the X-class flare. With the high quality vector magnetograms observed by the Hinode satellite, Schrijver *et al.* (2008) investigated the magnetic fields around the time of the X3.4 flare in AR 10930. They reconstructed the coronal magnetic structures by applying the nonlinear force-free field (NLFFF) modeling, and found that, before the flare, there were large currents at the initiation site of the X flare.

Magnetic shear is defined as the angular difference between the potential field and the observed field. Hagyard *et al.* (1984) quantitatively studied the magnetic shear along the PIL in an AR. Their results revealed that the shear angle was non-uniform along the PIL, and the maxima were at the locations of repeated flare onsets. They also suggested

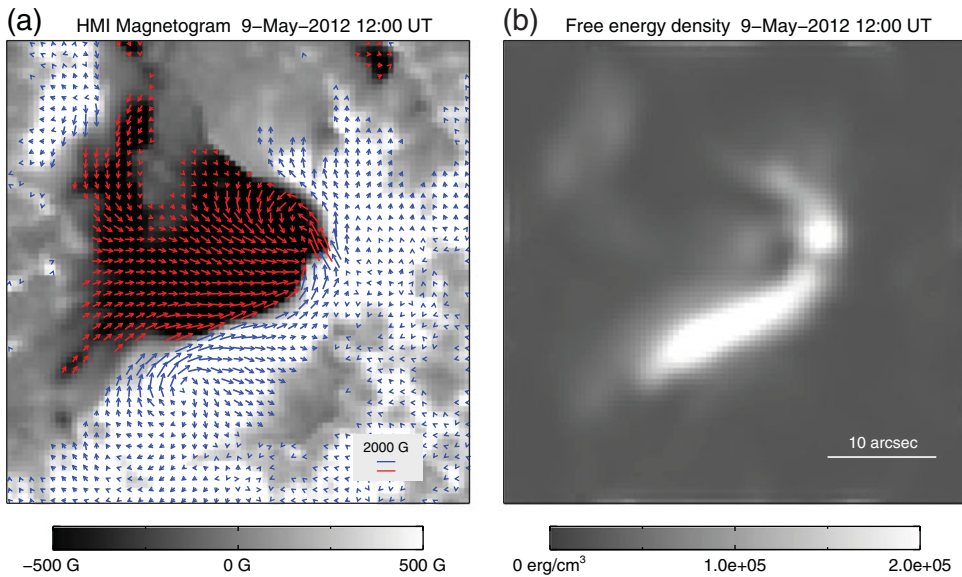


Figure 2. HMI vector magnetogram (panel (a)) and the calculated free energy density (panel (b)) before an M4.7 flare on 2012 May 09.

that continued magnetic field evolution caused the maximum shear to exceed a critical value, which resulted in a flare occurring around the site of maximum shear. AR 10486 is a super AR in solar cycle 23. It produced several major flares larger than X10 (i.e., X28, X17.2, X10) flares, in 2003. [Chen & Wang \(2012\)](#) quantified the characteristics of this AR using the vector magnetograms taken by the Solar Magnetic Field Telescope at HSOS. It is clear that, at the PIL, the free energy was quite high and the shear angles were very large. At some areas along the PIL, the shear angles were larger than 80 degrees. Fig. 2(a) displays the vector magnetic fields before an M4.7 flare on 2012 May 09 in AR 11476. We can see that the horizontal magnetic fields around the PIL are almost parallel to the PIL, and the highly sheared fields indicate that the magnetic fields are non-potential. Based on the vector field observation, the magnetic free energy density in the photosphere is calculated. The distribution of the free energy is displayed in Fig. 2(b). It reveals that the high free energy area (i.e., the bright region) is located along the PIL between the opposite polarities and corresponds to the initiation site of the M4.7 flare.

3. Photospheric dynamics

What have happened before the major flares? According to the previous studies, the emergence and cancellation of magnetic flux, the photospheric shearing motion, and the sunspot rotation are observed frequently.

Magnetic flux emergence and cancellation are thought to play an important role in triggering major flares and CMEs (e.g., [Zirin & Wang 1993](#); [Schmieder *et al.* 1997](#); [Choudhary *et al.* 1998](#); [Zhang *et al.* 2001](#); [Burtseva, & Petrie 2013](#)). [Wang & Shi \(1993\)](#) examined the associations of flares to flux emergence and cancellation. They found that the flux emergence and its driven flux cancellation with the pre-existing flux are one inseparable and elementary process, which is favorable for the occurrence of solar flares. [Zhang *et al.* \(2001\)](#) investigated the X5.7 flare on 2000 July 14 in AR 9077. After the detailed examination of the magnetic evolution, they found that the only obvious change was flux cancellation. The results indicated that the magnetic reconnection manifested as flux cancellation led to the global instability and thus resulted in the

major flare. [Burtseva, & Petrie \(2013\)](#) studied 77 X-class and M-class flares with the help of 1-minute cadence Global Oscillation Network Group (GONG) full-disk magnetograms, and the importance of flux cancellation in triggering major flares was proved. [Muhamad *et al.* \(2017\)](#) conducted 3-dimensional magnetohydrodynamic simulations, and suggested that the data-constrained simulation involving both the large-scale magnetic structure and small-scale disturbance, e.g., emerging flux, is efficient in discovering a flare-producing AR.

The rapid shearing flows in the photosphere are crucial in the buildup of free energy which can be released to power major solar flares ([Harvey & Harvey 1976](#); [Meunier & Kosovichev, \(2003\)](#); [Yang *et al.* 2004](#)). AR 10486 produced 8 X-class flares from 2003 October 23 to November 6. [Yang *et al.* \(2004\)](#) analyzed the high spatial resolution white-light observations with a 1 min cadence prior to an X10 flare in AR 10486, and found strong shearing flows along the PIL. These shearing flows were as high as 1.6 km s^{-1} , and they were well correlated with white-light flare kernels. With the observations from the Hinode, [Shimizu *et al.* \(2014\)](#) studied an X5.4 flare on 2012 March 7 and reported on a remarkable high-speed horizontal material flow along the PIL between two flare ribbons. The material flow was considered to contribute to increase the magnetic shear and to develop magnetic structures favorable for the flare initiation. In AR 11158, two emerging bipoles P1-N1 and P2-N2 collided against and sheared with each other and produced a highly sheared PIL, where the major flare kernel was located ([Toriumi *et al.* 2014](#)). [Park *et al.* \(2018\)](#) determined the photospheric shearing flows with a large data set of 2548 pairs of AR vector magnetograms, and investigated the shearing flows along strong magnetic PILs. They studied the relationship between the shearing flow parameters and the waiting time until the next major flare (M1.0 or above). Their results revealed that large ARs with widespread and/or strong shearing flows along PILs tend to produce major flares within 24 hr. Furthermore, [Chintzoglou *et al.* \(2019\)](#) demonstrated that the opposite polarities belonging to different bipolar magnetic regions collide, resulting in shearing and cancellation of magnetic flux, and named this kind of motion “collisional shearing”. [Fig. 3](#) shows a series of HMI intensity maps displaying the movements of two sunspots within AR 11476. The positive sunspot (marked with “P”) significantly sheared with the negative one (marked with “N”). During this process, several M-class flares occurred.

Besides shearing motion, sunspot rotation is also very important in the storage and release of free energy (e.g., [Stenflo 1969](#)). [Brown *et al.* \(2003\)](#) showed that some sunspots rotated up to 200 degrees around their center, and the corresponding coronal loops were twisted and finally erupted as flares. AR 10930 has been extensively studied (e.g., [Zhang *et al.* 2007](#); [Abramenko *et al.* 2008](#); [Min & Chae 2009](#); [Yan *et al.* 2009](#); [Inoue *et al.* 2012](#); [Bamba *et al.* 2013](#); [Gopasyuk 2015](#)). [Zhang *et al.* \(2007\)](#) examined the magnetic field and sunspot evolution in AR 10930. Around the PIL region, the interaction between the fast rotating sunspot and the ephemeral regions triggered a series of brightenings and eventually the major flare occurred. They also found that the major event took place after the sunspot rotated up to 200 degrees, and the sunspot rotated at least 240 degrees about its center. [Yan *et al.* \(2008\)](#) statistically studied the relationship between rotating sunspots and flare productivity, and found that the sunspots with the rotating direction opposite to the global differential rotation were in favor of producing strong flares. [Min & Chae \(2009\)](#) studied the pattern and behavior of a rotating sunspot in AR 10930 with the high-resolution G-band images from the Solar Optical Telescope onboard the Hinode, and examined the corresponding coronal structures using the Hinode/X-Ray Telescope images. They found that the small sunspot rotated about its center by 540 degrees during five days, and the coronal loops connecting two sunspots became sigmoidal in shape. In the simulation of [Amari *et al.* \(2014\)](#), due to the sunspot rotation and shearing motion, the field lines were twisted, forming a flux rope gradually.

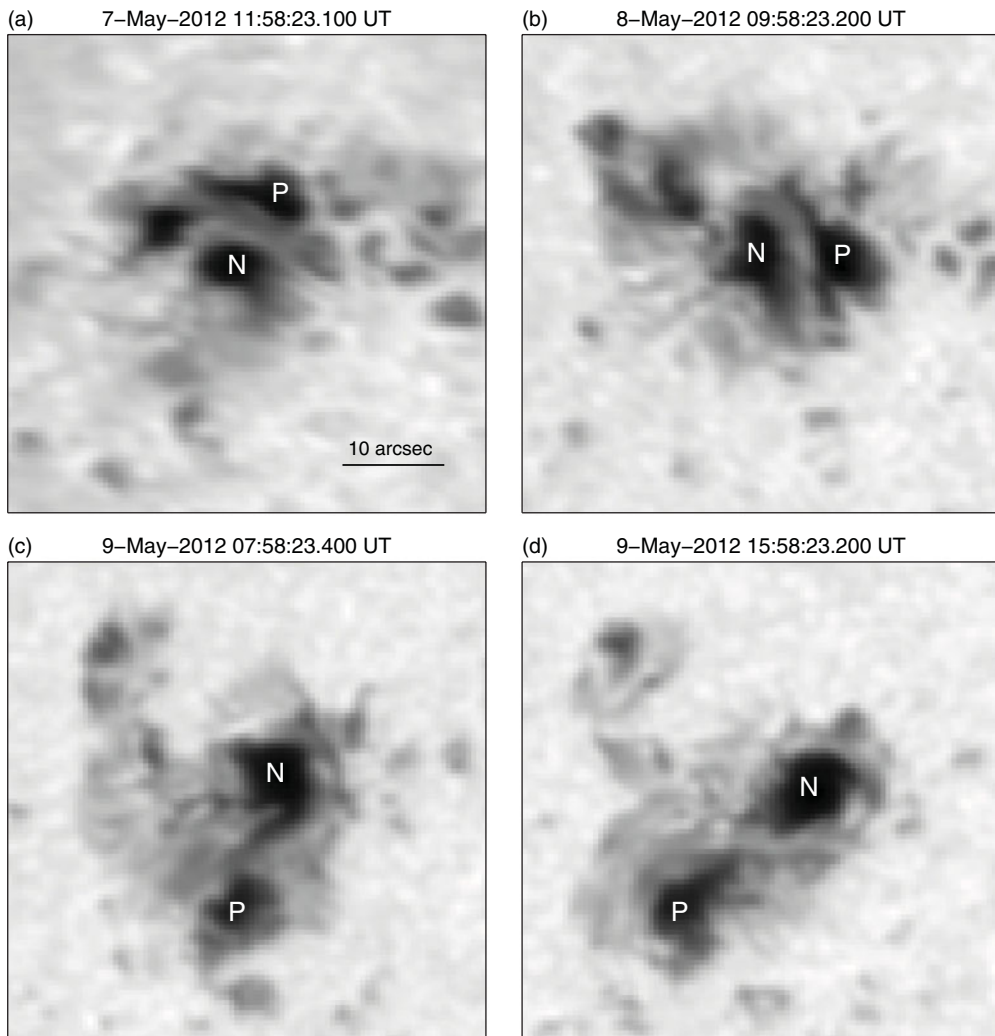


Figure 3. Sequence of HMI intensity maps showing the shearing motion of two sunspots with positive (marked with “P”) and negative (marked with “N”) polarities.

Then the flux rope erupted, triggering the X-class flare in AR 10930. [Vemareddy *et al.* \(2016\)](#) studied the major events in AR 12158 with the HMI vector magnetic field measurements and the AIA coronal EUV observations. It is shown that the time evolution of many non-potential parameters corresponded well with the sunspot rotation, and when the sunspots was rotating, two major eruptions occurred.

4. Flares and flux ropes

For the occurrence of solar flares, the CSHKP flare model has been well known for several decades ([Carmichael 1964](#); [Sturrock 1966](#); [Hirayama 1974](#); [Kopp & Pneuman 1976](#)). In the following years, solar flares have been observed and investigated in details with the development of the observational instruments. According to the popular flare model, a rising filament (flux rope) stretches the overlying loops, and a current sheet is created between the anti-directed field lines beneath the flux rope ([Shibata *et al.* 1995](#);

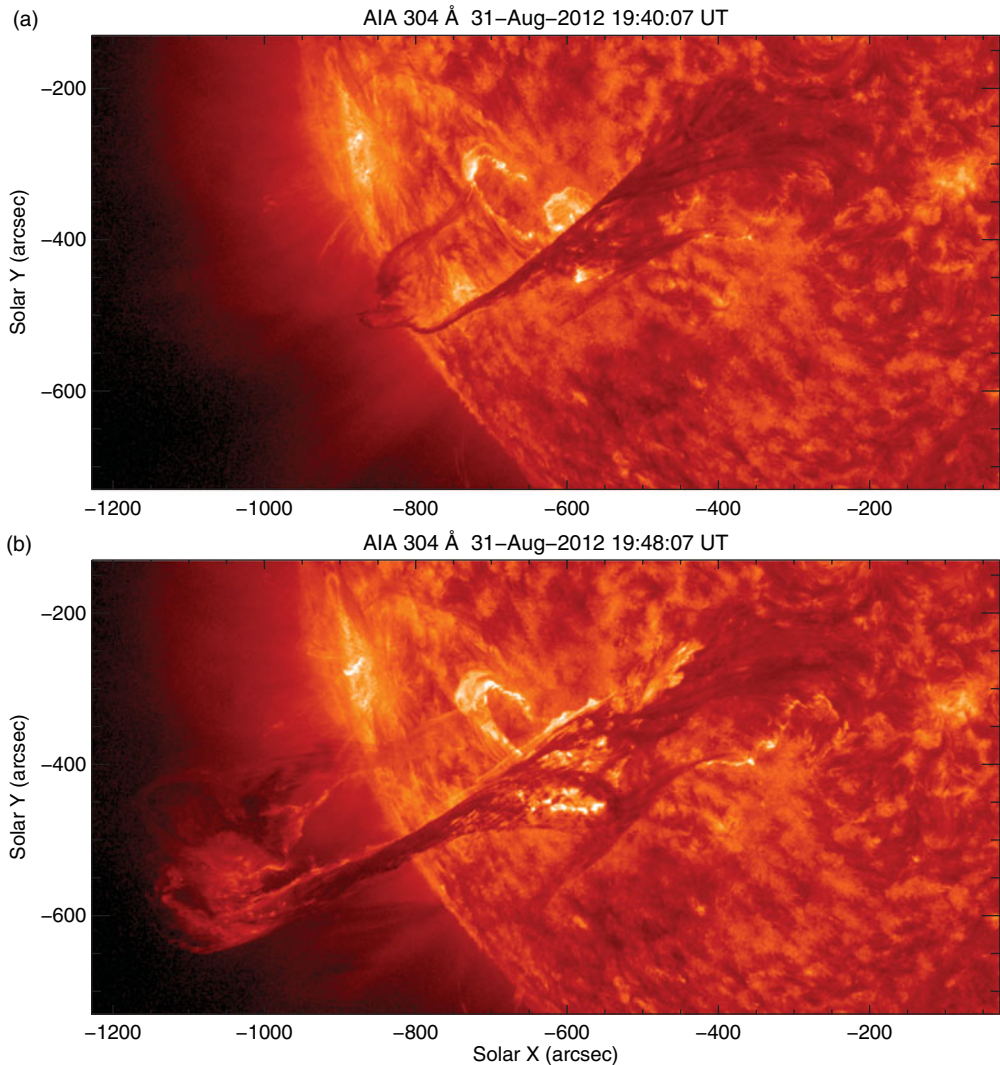


Figure 4. AIA 304 Å images showing a filament eruption accompanied by a two-ribbon flare on 2012 August 31.

Lin & Forbes 2000). Then magnetic reconnection takes place, and a solar flare occurs (Masuda *et al.* 1994). At the same time, the hot cusp-shaped coronal arcades are formed, and two ribbons at the feet of the coronal loops appear and separate. Fig. 4 shows a filament eruption observed in AIA 304 Å on 2012 August 31, which resulted in a two-ribbon flare. The eruption of the flux rope or the filament is often associated with a CME. The bright core of a CME always corresponds to the flux rope or the filament (Isenberg *et al.* 1993; Lin *et al.* 1998; Hudson *et al.* 2006).

Recently, an X8.2 flare event observed by SDO on 2017 September 10 is very consistent with the popular flare model (Fig. 5). In this event, a flux rope (denoted by the arrows in panels (a)-(b)) began to rise rapidly, behind which a long current sheet (denoted by the arrow in panel (c)) was formed. The width of the current sheet was estimated to be about 3000 km (Yan *et al.* 2018). Meanwhile, a cusp-shaped structure was formed due to the magnetic reconnection during the flare (see panel (d)). This event was also

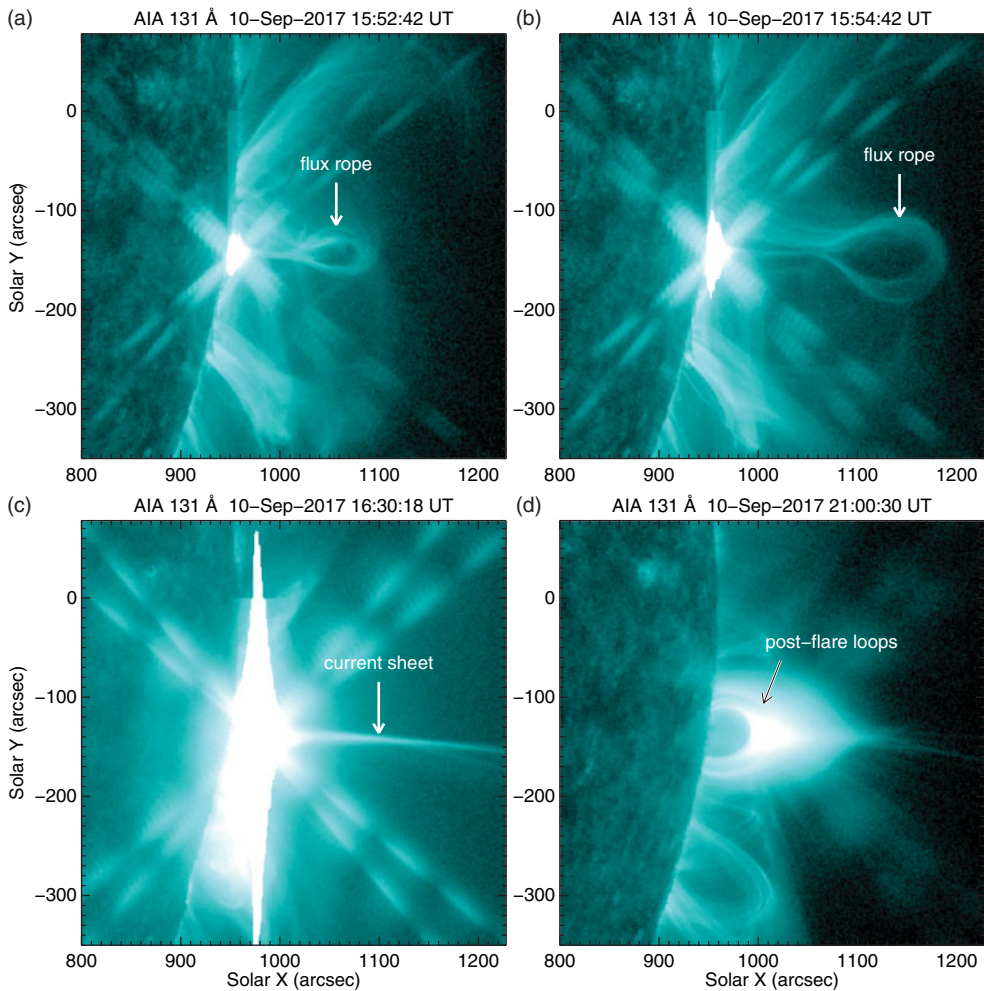


Figure 5. Sequence of AIA 131 Å images showing the occurrence of an X8.2 flare on 2017 September 10.

accompanied by a CME (Cheng *et al.* 2018). For this typical flare event, more details can be found in many papers (e.g., Hou *et al.* 2018; Li *et al.* 2018; Long *et al.* 2018; Seaton & Darnel 2018).

In ARs, the S shaped or inverse S shaped sigmoid structures in the corona are considered to be flux ropes (Rust & Kumar 1996; Canfield *et al.* 1999). If a flux rope is filled with dark material, it will be observed as a filament (Amari *et al.* 2000; Kleint *et al.* 2015). In a study of an M5.7 flare on 2012 May 10, Yang & Zhang (2018) reconstructed the coronal magnetic structures at the pre-flare stage using the NLFFF modeling (Wheatland *et al.* (2000); Wiegelmann (2004)). The results revealed that there was a flux rope above the PIL, which exactly corresponded to the H α filament observed with the ONSET.

In the images observed with the Atmospheric Imaging Assembly (AIA; Lemen *et al.* 2012) on board the SDO, some flux ropes only can be observed in high temperature line. In the study of Cheng *et al.* (2011) about an eruptive event on 2010 November 3 observed with AIA, a flux rope rapidly moving upward was seen as a bright blob of hot plasma in 131 Å passband. Zhang *et al.* (2012) studied a flux rope which was observed as a hot channel before and during a solar eruption with the AIA observations. The flux

rope initially appeared as a significantly twisted and writhed sigmoidal structure and its temperature was as high as 10 Mk. In a study about an erupting flux rope in AR 12733, [Yang *et al.* \(2019\)](#) determined the temperature of a flux rope with the Differential Emission Measure (DEM) method ([Cheung *et al.* 2015](#); [Su *et al.* 2018](#)). The results revealed that when the temperature range is as high as 10-40 MK, the flux rope is much brighter than the surrounding structures, which means that this flux rope is indeed a high-temperature structure.

However, some flux ropes cannot be observed in both lower and higher temperature lines. For example, [Li & Zhang \(2013\)](#) presented SDO observations of two flux ropes which were tracked out by surge and filament material. When the bright mass was added into the flux rope body, the flux ropes were detected. With the high spatial and temporal resolution NVST H α data, [Yang *et al.* \(2014\)](#) detected a flux rope tracked by activated filament material flow. Initially, the flux rope was invisible, and the filament material was located at one end of the flux rope. Then the filament was activated by magnetic flux cancellation. When the dark material flowed along helical threads, the twisted flux rope was tracked out.

Flux ropes can also be revealed by the shape of flare ribbons. For example, [Janvier *et al.* \(2014\)](#) paid attention to the double J-shaped flare ribbons during an eruptive X-class flare on 2011 February 15. They calculated the electric currents in the photosphere using the HMI vector magnetic field observations. The electric current in one ribbon was positive and in the other ribbon was negative. The shape of flare ribbons and the electric currents revealed how twisted the flux rope was in three dimensions.

When a flux rope becomes unstable, it will erupt. For the initiation of eruptions, there are several mechanisms. One possible mechanism is flux emergence ([Chen & Shibata 2000](#)). When magnetic flux emerges within the filament channel, it reconnects with the pre-existing magnetic field lines below the flux rope or on the outer edge of the filament channel, leading to the loss of equilibrium. Then the flux rope rises, a current sheet below it is formed. The fast reconnection in the current sheet induces the fast ejection of the flux rope.

Another mechanism is the tether cutting based on a single bipolar field geometry ([Moore *et al.* 2001](#)). In the tether cutting model, the highly sheared core fields are overlaid by magnetic arcades. The sheared fields slowly reconnect above the PIL, forming a large-scale twisted flux rope and some small shrinking flaring loops. The reconnection beneath the flux rope cuts off the anchoring of field lines, and allows the flux rope to rise and erupt. [Chen *et al.* \(2014\)](#) investigated an X4.9 flare in AR 11990 and reported the observation of tether cutting reconnection between pre-existing loops. Prior to the X4.9 flare, some pre-existing loops interacted with each other, producing a brightening region beneath the filament. Below the interaction region, a small flaring loop appeared. Meanwhile, some large-scale new helical field lines connecting two far ends of the loop structures were formed and added into the former twisted flux rope. Then due to the imbalance between the magnetic pressure and magnetic tension, the newly formed flux rope together with the filament erupted outward. This process coincides well with the tether cutting model.

A similar model is the magnetic breakout model in a multi-polar magnetic configuration ([Antiochos 1998](#); [Antiochos *et al.* \(1999\)](#)). It can be regarded as the external tether cutting. In the breakout model, the reconnection occurs high in the corona above a flux rope. Since the reconnection takes between the central flux rope and the overlying field, the confinement from the overlying magnetic field is removed, like an onion-peeling process. Consequently, the flux rope begins to rise and erupt outward. [Chen *et al.* \(2016\)](#) reported critical observational evidence of breakout reconnection leading to an X-class

flare and a CME. The observations clearly showed the presence of pairs of heated cusp-shaped loops around an X-type null point. In addition, there also existed signatures of reconnection inflows.

For a flux rope, there is a critical twist, above which the flux rope is unstable. This kind of instability is called kink instability (Hood & Priest 1979; Török & Kliem 2003, Török & Kliem 2005). The typical threshold value of the twist needed for kink instability under coronal conditions is about 3.5π , equivalent to 1.75 turns. Kumar *et al.* (2012) presented multi-wavelength AIA observations of an M3.5 limb flare associated with a CME triggered by the helical kink instability on 2011 February 24 in AR 11163. The event in their study is in agreement with the standard flare model (CSHKP). The twist of the flux rope is estimated to be 6π – 8π , which is sufficient to generate the kink instability.

If the background field above a flux rope decays fast enough, the flux rope is unstable. This kind of instability is called torus instability (Kliem & Török 2006). The critical value for the torus instability is given by

$$n = -\frac{d(\log B)}{d(\log R)} > 1.5, \quad (4.1)$$

where B is the strength of the background field at a geometrical height R above the eruption site. If the decay index (n) approaches the threshold, it will result in torus instability or partial torus instability (Aulanier *et al.* 2010; Démoulin & Aulanier 2010; Olmedo & Zhang 2010).

5. The largest flare in solar cycle 24

In 2017 September, AR 12673 produced a series of flares, including 31 major flares (4 X-class and 27 M-class flares), from September 4 to 10. After the first publication (Yang *et al.* 2017) about this super AR, a lot of more studies have been carried out (e.g., Sun & Norton 2017; Wang *et al.* 2018, Wang *et al.* 2018; Chertok 2018; Yan *et al.* 2018; Sharykin & Kosovichev 2018; Hou *et al.* 2018; Inoue *et al.* 2018; Jiang *et al.* 2018; Zou *et al.* 2019; Li *et al.* 2019; Romano *et al.* 2019; Vemareddy 2019; Getling 2019; Moraitis *et al.* 2019; Price *et al.* 2019; Anfinogentov *et al.* 2019).

Among the numerous flares in AR 12673, the X9.3 flare (Fig. 6) is the largest one in solar cycle 24. Yang *et al.* (2017) mainly focused on two questions: (1) Why was this AR so flare-productive? (2) How did the largest flare occur? In the HMI intensity maps, there was only one sunspot in the initial several days (see Fig. 1 in Yang *et al.* 2017). Then two bipoles “A” and “B” emerged nearby it successively. Due to the standing of the pre-existing sunspot, the movement of the bipoles was blocked. Thus, the bipolar patches were greatly distorted. The opposite polarities formed two semi-circular shaped structures. Then two new bipoles “C” and “D” emerged within the semi-circular zone. The newly emerging bipolar patches separated along the curved channel, and interacted with the previous fields, forming a complex system. During this process, numerous flares occurred. As noted by Sun & Norton (2017), this AR has one of the fastest magnetic flux emergence ever observed. They calculated the magnetic flux emergence rate in 6-hr chunks, and found the instantaneous magnetic flux emergence rate around 21:00 UT on September 3 was as high as $1.12_{-0.05}^{+0.15} \times 10^{21}$ Mx hr⁻¹, which occurred during the early emerging stage.

At the PIL, the magnetic fields were highly sheared, and a great deal of free magnetic energy was stored. Based on the observed photospheric vector magnetograms, Yang *et al.* (2017) extrapolated the coronal magnetic fields using the NLFFF modeling. Moreover, using the code developed by Liu *et al.* (2016), Yang *et al.* (2017) calculated the twist number T_w (Berger & Prior 2006) and squashing factor Q (Demoulin *et al.* 1996;

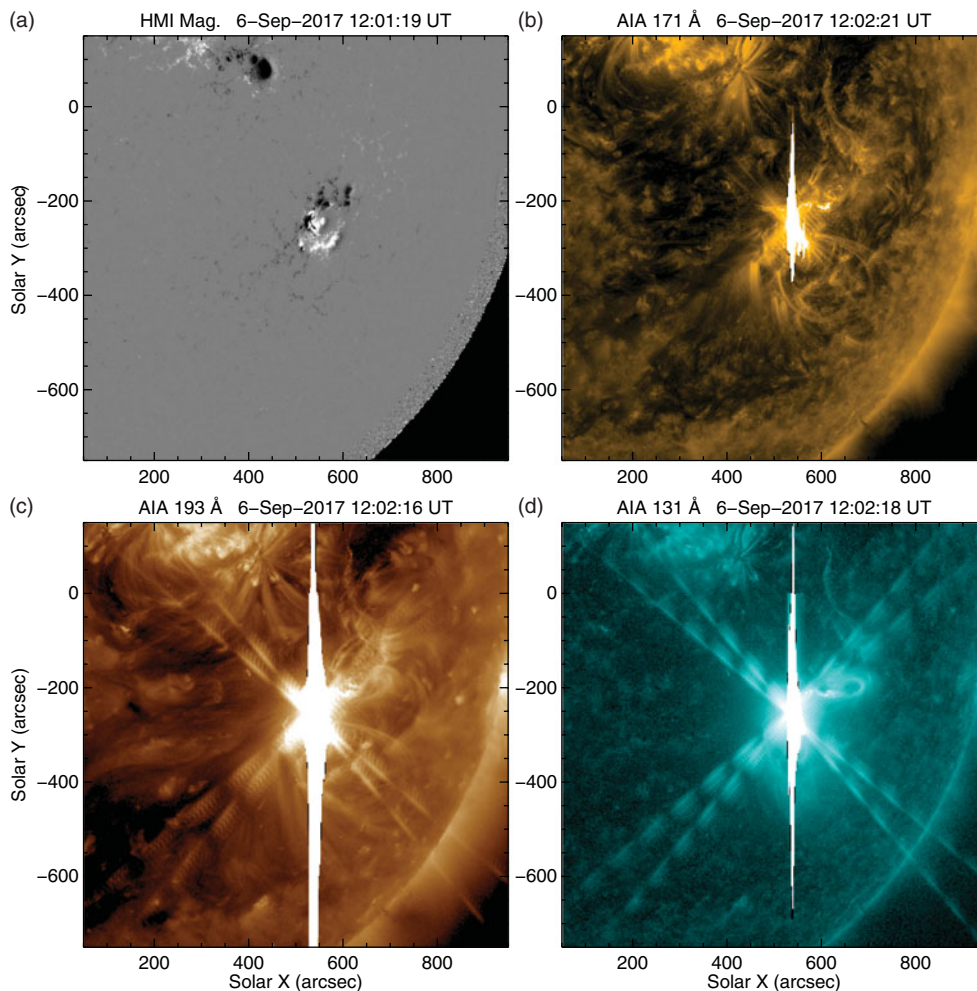


Figure 6. HMI magnetogram (panel (a)), AIA 171 Å (panel (b)), 193 Å (panel (c)), and 131 Å (panel (d)) images showing the appearance of an X9.3 flare on 2017 September 6 in AR 12673.

Titov *et al.* (2002)) of the reconstructed coronal magnetic field. The reconstructed magnetic structures revealed that there was a flux rope above the PIL, as shown by the red structure (Fig. 7). About 2 hr before the X9.3 flare, the average T_w of the inner part of the flux rope was about -1.5 .

To examine the magnetic gradient across the main PIL at the AR core, Mitra *et al.* (2018) considered a slit across the PIL. Along the slit, magnetic field strength and gradient were calculated. They found that the magnetic field gradient was very sharp. The magnetic strength changes from -1000 G to 1000 G over a distance of about 1 arcsec, with the peak gradient of about 2.4×10^3 G Mm $^{-1}$ on the PIL. With the 0.1 arcsec spatial resolution observations obtained by the GST at BBSO, Wang *et al.* (2018) found that the light bridge within this AR has usual behaviors, i.e., the strong magnetic fields and apparent photospheric twist.

At the core of the AR, the positive and negative fields sheared with each other continually. In addition, the sunspot with negative polarity rotated anticlockwise. Therefore, the twist number T_w of the flux rope continuously increased, which ultimately reached

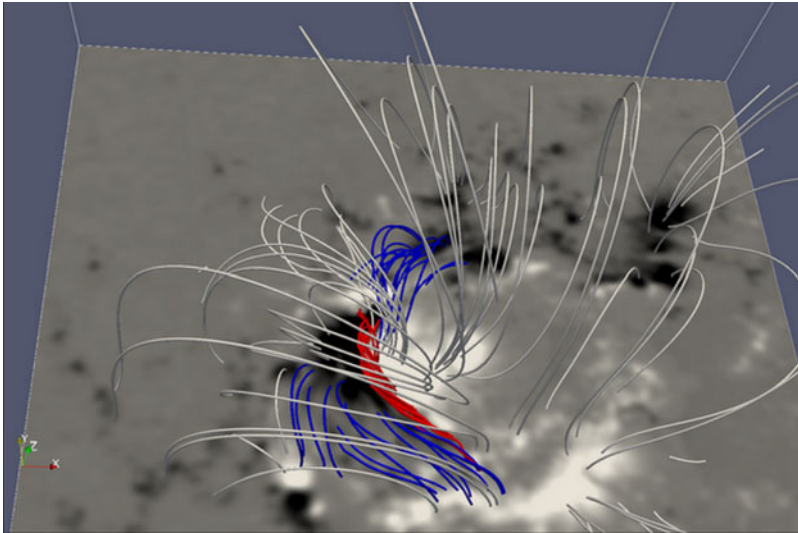


Figure 7. Side-view of the 3-dimensional coronal structures reconstructed from the HMI photospheric vector magnetogram before the X9.3 flare on 2017 September 6.

or even exceeded the threshold of the kink instability. AIA images clearly show that a filament erupted and two ribbons appeared. The observed filament in AIA 304 Å images corresponds to the reconstructed flux rope using the NLFFF method. During the filament eruption, a kink structure appeared (Yang *et al.* 2017). It is a signature of the kink instability, which triggered the largest flare.

Based on the observations, Yang *et al.* (2017) proposed for the first time the block-induced eruption model to answer the two main questions. In this model, there was a standing sunspot, which blocked the movement of newly emerging bipoles. The block-induced complex structures built the flare-productive AR, and the X9.3 flare was triggered by an erupting flux rope due to the kink instability. When the flux rope erupted, it interacted with two nearby flux ropes (Hou *et al.* 2018; Mitra *et al.* 2018). Eventually, the multi-flux-rope system erupted outward, forming a CME.

Acknowledgements

The data are used courtesy of NVST, HMI, AIA, and GOES science teams. This work is supported by the National Natural Science Foundations of China (11673035, 11790304, 11533008, 11790300), Key Programs of the Chinese Academy of Sciences (QYZDJ-SSW-SLH050), and the Youth Innovation Promotion Association of CAS.

References

- Abramenko, V., Yurchyshyn, V., & Wang, H. 2008, *Astrophys. J.*, 681, 1669
 Amari, T., Luciani, J. F., Mikic, Z., & Linker, J. 2000, *Astrophys. J. Lett.*, 529, L49
 Amari, T., Canou, A., & Aly, J.-J. 2014, *Nature*, 514, 465
 Anfinogentov, S. A., Stupishin, A. G., Myshyakov, I. I., & Fleishman, G. D. 2019, *Astrophys. J. Lett.*, 880, L29
 Antiochos, S. K. 1998, *Astrophys. J. Lett.*, 502, L181
 Antiochos, S. K., DeVore, C. R., & Klimchuk, J. A. 1999, *Astrophys. J.*, 510, 485
 Aulanier, G., Török, T., Démoulin, P., & DeLuca, E. E. 2010, *Astrophys. J.*, 708, 314
 Bamba, Y., Kusano, K., Yamamoto, T. T., *et al.* 2013, *Astrophys. J.*, 778, 48
 Benz, A. O., & Krucker, S. 1998, *Sol. Phys.*, 182, 349

- Benz, A. O. 2017, *Living Rev. Sol. Phys.*, 14, 2
- Berger, M. A., & Prior, C. 2006, *J. Phys. A*, 39, 8321
- Berghmans, D., Clette, F., & Moses, D. 1998, *Astron. Astrophys.*, 336, 1039
- Brown, D. S., Nightingale, R. W., Alexander, D., et al. 2003, *Sol. Phys.*, 216, 79
- Burtseva, O., & Petrie, G. 2013, *Sol. Phys.*, 283, 429
- Canfield, R. C., Hudson, H. S., & McKenzie, D. E. 1999, *Geophys. Res. Lett.*, 26, 627
- Cao, W., Gorceix, N., Coulter, R., et al. 2010, *Astro. Nachr.*, 331, 636
- Carmichael, H. 1964, *NASA Special Publication*, 50, 451
- Carrington, R. C. 1859, *Mon. Not. Roy. Astron. Soc.*, 20, 13
- Chen, A. Q., & Wang, J. X. 2012, *Astron. Astrophys.*, 543, A49
- Chen, H., Zhang, J., Cheng, X., et al. 2014, *Astrophys. J. Lett.*, 797, L15
- Chen, P. F. 2011, *Living Rev. Sol. Phys.*, 8, 1
- Chen, P. F., & Shibata, K. 2000, *Astrophys. J.*, 545, 524
- Chen, X., Yan, Y., Tan, B., et al. 2019, *Astrophys. J.*, 878, 78
- Chen, Y., Du, G., Zhao, D., et al. 2016, *Astrophys. J. Lett.*, 820, L37
- Cheng, X., Li, Y., Wan, L. F., et al. 2018, *Astrophys. J.*, 866, 64
- Cheng, X., Zhang, J., Liu, Y., et al. 2011, *Astrophys. J. Lett.*, 732, L25
- Chertok, I. M. 2018, *Res. Notes AAS*, 2, 20
- Cheung, M. C. M., Boerner, P., Schrijver, C. J., et al. 2015, *Astrophys. J.*, 807, 143
- Chintzoglou, G., Zhang, J., Cheung, M. C. M., et al. 2019, *Astrophys. J.*, 871, 67
- Choudhary, D. P., Ambastha, A., & Ai, G. 1998, *Sol. Phys.*, 179, 133
- De Pontieu, B., Title, A. M., Lemen, J. R., et al. 2014, *Sol. Phys.*, 289, 2733
- Demoulin, P., Henoux, J. C., Priest, E. R., & Mandrini, C. H. 1996, *Astron. Astrophys.*, 308, 643
- Démoulin, P., & Aulanier, G. 2010, *Astrophys. J.*, 718, 1388
- Domingo, V., Fleck, B., & Poland, A. I. 1995, *Sol. Phys.*, 162, 1
- Fang, C., Chen, P.-F., Li, Z., et al. 2013, *Res. Astron. Astrophys.*, 13, 1509–1517
- Getling, A. V. 2019, *Astrophys. J.*, 878, 127
- Gopasyuk, O. S. 2015, *Adv. Space Res.*, 55, 937
- Hagyard, M. J., Smith, J. B., Jr., Teuber, D., & West, E. A. 1984, *Sol. Phys.*, 91, 115
- Haisch, B., Strong, K. T., & Rodono, M. 1991, *Annu. Rev. Astron. Astrophys.*, 29, 275
- Harvey, K. L., & Harvey, J. W. 1976, *Sol. Phys.*, 47, 233
- Hirayama, T. 1974, *Sol. Phys.*, 34, 323
- Hodgson, R. 1859, *Mon. Not. Roy. Astron. Soc.*, 20, 15
- Hood, A. W., & Priest, E. R. 1979, *Sol. Phys.*, 64, 303
- Hou, Y. J., Zhang, J., Li, T., et al. 2018, *Astron. Astrophys.*, 619, A100
- Hudson, H. S., Bougeret, J.-L., & Burkepile, J. 2006, *Space Sci. Rev.*, 123, 13
- Inoue, S., Shiota, D., Yamamoto, T. T., et al. 2012, *Astrophys. J.*, 760, 17
- Inoue, S., Shiota, D., Bamba, Y., & Park, S.-H. 2018, *Astrophys. J.*, 867, 83
- Isenberg, P. A., Forbes, T. G., & Demoulin, P. 1993, *Astrophys. J.*, 417, 368
- Jaeggli, S. A. 2016, *Astrophys. J.*, 818, 81
- Janvier, M., Aulanier, G., Bommier, V., et al. 2014, *Astrophys. J.*, 788, 60
- Jiang, C., Zou, P., Feng, X., et al. 2018, *Astrophys. J.*, 869, 13
- Jing, J., Song, H., Abramenko, V., Tan, C., & Wang, H. 2006, *Astrophys. J.*, 644, 1273
- Kilpua, E., Koskinen, H. E. J., & Pulkkinen, T. I. 2017, *Living Rev. Sol. Phys.*, 14, 5
- Kleint, L., Battaglia, M., Reardon, K., et al. 2015, *Astrophys. J.*, 806, 9
- Kliem, B., & Török, T. 2006, *Phys. Rev. Lett.*, 96, 255002
- Kopp, R. A., & Pneuman, G. W. 1976, *Sol. Phys.*, 50, 85
- Kosugi, T., Matsuzaki, K., Sakao, T., et al. 2007, *Sol. Phys.*, 243, 3
- Kumar, P., Cho, K.-S., Bong, S.-C., Park, S.-H., & Kim, Y. H. 2012, *Astrophys. J.*, 746, 67
- Lemen, J. R., Title, A. M., Akin, D. J., et al. 2012, *Sol. Phys.*, 275, 17
- Li, T., & Zhang, J. 2013, *Astrophys. J. Lett.*, 770, L25
- Li, X., Zhang, J., Yang, S., & Hou, Y. 2019, *Publ. Astron. Soc. Jpn.*, 71, 14
- Li, Y., Xue, J. C., Ding, M. D., et al. 2018, *Astrophys. J. Lett.*, 853, L15

- Lin, J., & Forbes, T. G. 2000, *J. Geophys. Res-Space Phys.*, 105, 2375
- Lin, J., Forbes, T. G., Isenberg, P. A., & Démoulin, P. 1998, *Astrophys. J.*, 504, 1006
- Lin, R. P., Dennis, B. R., Hurford, G. J., et al. 2002, *Sol. Phys.*, 210, 3
- Liu, R., Kliem, B., Titov, V. S., et al. 2016, *Astrophys. J.*, 818, 148
- Liu, Z., Xu, J., Gu, B.-Z., et al. 2014, *Res. Astron. Astrophys.*, 14, 705–718
- Long, D. M., Harra, L. K., Matthews, S. A., et al. 2018, *Astrophys. J.*, 855, 74
- Masuda, S., Kosugi, T., Hara, H., Tsuneta, S., & Ogawara, Y. 1994, *Nature*, 371, 495
- Meunier, N., & Kosovichev, A. 2003, *Astron. Astrophys.*, 412, 541
- Min, S., & Chae, J. 2009, *Sol. Phys.*, 258, 203
- Mitra, P. K., Joshi, B., Prasad, A., et al. 2018, *Astrophys. J.*, 869, 69
- Moore, R. L., Sterling, A. C., Hudson, H. S., et al. 2001, *Astrophys. J.*, 552, 833
- Moraitis, K., Sun, X., Pariat, É., & Linan, L. 2019, *Astron. Astrophys.*, 628, A50
- Muhamad, J., Kusano, K., Inoue, S., & Shiota, D. 2017, *Astrophys. J.*, 842, 86
- Olmedo, O., & Zhang, J. 2010, *Astrophys. J.*, 718, 433
- Okamoto, T. J., & Sakurai, T. 2018, *Astrophys. J. Lett.*, 852, L16
- Park, S.-H., Guerra, J. A., Gallagher, P. T., Georgoulis, M. K., & Bloomfield, D. S. 2018, *Sol. Phys.*, 293, 114
- Parker, E. N. 1957, *J. Geophys. Res-Space Phys.*, 62, 509
- Pesnell, W. D., Thompson, B. J., & Chamberlin, P. C. 2012, *Sol. Phys.*, 275, 3
- Price, D. J., Pomoell, J., Lumme, E., & Kilpua, E. K. J. 2019, *Astron. Astrophys.*, 628, A114
- Priest, E. R., & Forbes, T. G. 2002, *Astron. Astrophys. Rev.*, 10, 313
- Pulkkinen, T. 2007, *Living Rev. Sol. Phys.*, 4, 1
- Régnier, S., & Canfield, R. C. 2006, *Astron. Astrophys.*, 451, 319
- Romano, P., Elmhamdi, A., & Kordi, A. S. 2019, *Sol. Phys.*, 294, 4
- Rosner, R., Golub, L., & Vaiana, G. S. 1985, *Annu. Rev. Astron. Astrophys.*, 23, 413
- Rust, D. M., & Kumar, A. 1996, *Astrophys. J. Lett.*, 464, L199
- Scherrer, P. H., Schou, J., Bush, R. I., et al. 2012, *Sol. Phys.*, 275, 207
- Schmieder, B., Aulanier, G., Demoulin, P., et al. 1997, *Astron. Astrophys.*, 325, 1213
- Schmieder, B., Aulanier, G., & Vršnak, B. 2015, *Sol. Phys.*, 290, 3457
- Schou, J., Scherrer, P. H., Bush, R. I., et al. 2012, *Sol. Phys.*, 275, 229
- Schrijver, C. J. 2007, *Astrophys. J. Lett.*, 655, L117
- Schrijver, C. J., DeRosa, M. L., Metcalf, T., et al. 2008, *Astrophys. J.*, 675, 1637
- Schwenn, R. 2006, *Living Rev. Sol. Phys.*, 3, 2
- Seaton, D. B., & Darnel, J. M. 2018, *Astrophys. J. Lett.*, 852, L9
- Sharykin, I. N., & Kosovichev, A. G. 2018, *Astrophys. J.*, 864, 86
- Shibata, K., Masuda, S., Shimojo, M., et al. 1995, *Astrophys. J. Lett.*, 451, L83
- Shimizu, T., Lites, B. W., & Bamba, Y. 2014, *Publ. Astron. Soc. Jpn.*, 66, S14
- Song, Q., Zhang, J., Yang, S.-H., et al. 2013, *Res. Astron. Astrophys.*, 13, 226
- Stenflo, J. O. 1969, *Sol. Phys.*, 8, 115
- Sturrock, P. A. 1966, *Nature*, 211, 695
- Su, Y., Veronig, A. M., Hannah, I. G., et al. 2018, *Astrophys. J. Lett.*, 856, L17
- Sun, X., Hoeksema, J. T., Liu, Y., et al. 2012, *Astrophys. J.*, 748, 77
- Sun, X., & Norton, A. A. 2017, *Res. Notes AAS*, 1, 24
- Titov, V. S., Hornig, G., & Démoulin, P. 2002, *J. Geophys. Res-Space Phys.*, 107, 1164
- Toriumi, S., Iida, Y., Kusano, K., et al. 2014, *Sol. Phys.*, 289, 3351
- Toriumi, S., Schrijver, C. J., Harra, L. K., et al. 2017, *Astrophys. J.*, 834, 56
- Toriumi, S., & Wang, H. 2019, *Living Rev. Sol. Phys.*, 16, 3
- Török, T., & Kliem, B. 2003, *Astron. Astrophys.*, 406, 1043
- Török, T., & Kliem, B. 2005, *Astrophys. J. Lett.*, 630, L97
- Vemareddy, P. 2019, *Astrophys. J.*, 872, 182
- Vemareddy, P., Ambastha, A., & Maurya, R. A. 2012, *Astrophys. J.*, 761, 60
- Vemareddy, P., Cheng, X., & Ravindra, B. 2016, *Astrophys. J.*, 829, 24
- Wang, H., & Liu, C. 2015, *Res. Astron. Astrophys.*, 15, 145–174
- Wang, H., Yurchyshyn, V., Liu, C., et al. 2018a, *Res. Notes AAS*, 2, 8

- Wang, J., & Shi, Z. 1993, *Sol. Phys.*, 143, 119
- Wang, J., Shi, Z., Wang, H., *et al.* 1996, *Astrophys. J.*, 456, 861
- Wang, R., Liu, Y. D., Hoeksema, J. T., Zimovets, I. V., & Liu, Y. 2018b, *Astrophys. J.*, 869, 90
- Wheatland, M. S., Sturrock, P. A., & Roumeliotis, G. 2000, *Astrophys. J.*, 540, 1150
- Wiegelmann, T. 2004, *Sol. Phys.*, 219, 87
- Yan, X.-L., Qu, Z.-Q., & Kong, D.-F. 2008, *Mon. Not. Roy. Astron. Soc.*, 391, 1887
- Yan, X.-L., Qu, Z.-Q., Xu, C.-L., *et al.* 2009, *Res. Astron. Astrophys.*, 9, 596
- Yan, X. L., Wang, J. C., Pan, G. M., *et al.* 2018, *Astrophys. J.*, 856, 79
- Yan, X. L., Yang, L. H., Xue, Z. K., *et al.* 2018, *Astrophys. J. Lett.*, 853, L18
- Yan, Y., Zhang, J., Wang, W., *et al.* 2009, *Earth Moon Planets*, 104, 97
- Yan, Y., Chen, L., & Yu, S. 2016, IAU Symp. 320 in *Solar and Stellar Flares and their Effects on Planets*, ed. A. G. Kosovichev, S. L. Hawley, & P. Heinzel (Cambridge: Cambridge Univ. Press), 427
- Yang, G., Xu, Y., Cao, W., *et al.* 2004, *Astrophys. J. Lett.*, 617, L151
- Yang, S., & Zhang, J. 2018, *Astrophys. J. Lett.*, 860, L25
- Yang, S., Zhang, J., Liu, Z., & Xiang, Y. 2014b, *Astrophys. J. Lett.*, 784, L36
- Yang, S., Zhang, J., Song, Q., Bi, Y., & Li, T. 2019, *Astrophys. J.*, 878, 38
- Yang, S., Zhang, J., & Xiang, Y. 2014a, *Astrophys. J. Lett.*, 793, L28
- Yang, S., Zhang, J., & Xiang, Y. 2015, *Astrophys. J. Lett.*, 798, L11
- Yang, S., Zhang, J., Zhu, X., & Song, Q. 2017, *Astrophys. J. Lett.*, 849, L21
- Zhang, J., Wang, J., Deng, Y., & Wu, D. 2001, *Astrophys. J. Lett.*, 548, L99
- Zhang, J., Li, L., & Song, Q. 2007, *Astrophys. J. Lett.*, 662, L35
- Zhang, J., Cheng, X., & Ding, M.-D. 2012, *Nat. Commun.*, 3, 747
- Zirin, H., & Wang, H. 1993, *Nature*, 363, 426
- Zirin, H., & Wang, H. 1993, *Sol. Phys.*, 144, 37
- Zou, P., Jiang, C., Feng, X., *et al.* 2019, *Astrophys. J.*, 870, 97

Discussion

K. STRASSMEIER: Do you see a relation to radio-II bursts along with X-class flares?

S. YANG: For these X-class flares, we have not paid attention to the radio-II bursts. It is indeed worth studying.

J. LUHMANN: Given the obvious complexity of the initiation of the flare you describe, what advice would you have for the flare forecasting community?

S. YANG: Magnetic field is the most important factor for the flare initiation, and now only the magnetic field in the photosphere can be accurately measured. If we want to forecast the flare occurrence, we should focus on the structure and evolution of the photospheric magnetic field. We can examine the complexity of the vector magnetograms of active regions, e.g., the polarity-inversion lines with strong shear angles. In addition, we can examine the photospheric evolution, especially the significant flux emergence and sunspot rotation.

Y. YAN: You showed the largest flare processes in solar cycle 24. There was also a largest sunspot produced many X-class flares and there were not many CMEs accompanied. Do you compare any difference between these two event?

S. YANG: The largest sunspot group in solar cycle 24 is within active region 12192 in 2014 October. It produced 6 X-class flares and none of them was accompanied by CME. This is mainly due to the strong confinement from the overlying field above the flaring core region of active region 12192.